Available online at *www.ujpronline.com*
Universal Journal of Pharmaceutical Research
An International Peer Reviewed Journal
ISSN: 2831-5235 (Print); 2456-8058 (Electronic)

RESEARCH ARTICLE

MOLECULAR MODELING AND VIRTUAL SCREENING FOR COMPUTER-AIDED DESIGN OF HCV NS5B POLYMERASE INHIBITORS

Bertrand-Ulrich Yavo[1], Akori Elvice Esmel[1], Kouakou Jean-Louis Kouakou[1], Melalie Kéita[1], Megnassan Eugène[1,2*]

[1]Laboratory of Fundamental and Applied Physics, UFR SFA, Nangui Abrogoua University, BP 801 Abidjan 02, Côte d'Ivoire.
[2]ICTP-UNESCO, QLS, Strada Costiera, 11, I-34151, Trieste, Italy.

Article Info:

Article History:
Received: 5 April 2026
Reviewed: 13 May 2026
Accepted: 10 June 2026
Published: 15 July 2026

Cite this article:
Yavo BU, Esmel AE, Kouakou KJL, Kéita M, Eugène M. Molecular modeling and virtual screening for computer-aided design of HCV NS5B polymerase inhibitors. Universal journal of pharmaceutical research 2026; 11(3): 43-57.
http://doi.org/10.22270/ujpr.v11i3.1586

***Address for Correspondence:**
Dr. Megnassan Eugène, Laboratory of Fundamental and Applied Physics, UFR SFA, Nangui Abrogoua University, BP 801 Abidjan 02, Côte d'Ivoire. 2ICTP-UNESCO, QLS, Strada Costiera, 11, I-34151, Trieste, Italy. Mobile: +225-02363008;
E-mail: *megnase@gmail.com*

Abstract

Aims and objectives: This study aims to design new inhibitors for the Hepatitis C Virus (HCV) Non-Structural Protein 5B (NS5B) polymerase, an enzyme essential for viral replication. The research addresses an urgent public health issue affecting 71 million people and causing approximately 242,000 deaths annually.
Methodology: The research follows a computer-aided rational design approach. A Quantitative Structure-Activity Relationship (QSAR) model was developed using 24 quinazolinone derivatives (QDs) to correlate Gibbs free energy with experimental inhibition constants. The bound conformations of the ligands were used to construct a 3D-QSAR pharmacophore (PH4) model. A virtual library of 168,750 QDs was generated and filtered using ADME (Absorption, Distribution, Metabolism, and Excretion) criteria and PH4 screening. Conformational stability was evaluated through 200-ns molecular dynamics (MD) simulations. Binding free energy variations were quantified using the Molecular Mechanics - Generalized Born Surface Area (MM-GBSA) approach on MD trajectories, calculating molecular mechanics energy, solvation energy, and surface area contributions under the OPLS2005 force field.
Results: The QSAR model showed high predictive power and the PH4 model achieved an R^2 of 0.85. Screening identified 39 potent analogues. The lead candidate, 3-6-4-45, exhibited a predicted inhibitory concentration of 0.62 nM, approximately 96 times more active than the best reference ligand (60 nM). MD simulations confirmed stability with RMSD values between 1.5 and 3 Å. MM-GBSA binding energies converged with predicted complexation energies, validating the computational reliability.
Conclusion: The integration of molecular modeling and *in silico* screening successfully identified six potent candidate inhibitors of the HCV NS5B polymerase with favorable pharmacokinetic profiles. These analogues represent high-affinity candidates for future therapeutic development.
Keywords: Computer-aided rational design, inhibitors, molecular dynamics, NS5B polymerase, pharmacophore, QSAR, quinazolinone derivatives, virtual screening.

INTRODUCTION

The liver is an essential organ that performs vital physiological functions. Its impairment by chronic viral infections, such as the hepatitis C virus (HCV), leads to severe conditions, including cirrhosis and hepato-cellular carcinoma[1]. HCV remains a significant global public health issue, affecting approximately 71 million individuals and resulting in hundreds of thousands of deaths annually due to liver-related complications[2]. Despite the clinical success of current Direct-Acting Antivirals (DAAs), the extreme genetic variability of HCV and the rapid emergence of drug-resistant mutations create a shifting therapeutic landscape. This constant viral evolution can compromise even highly effective regimens, necessitating continuous efforts to develop novel, resilient therapeutic strategies[3].

Focusing on replicative enzymes, especially the NS5B polymerase, which is an RNA-dependent RNA polymerase crucial for the replication of the viral genome, is a well-established and highly promising strategy[4]. By inhibiting NS5B, the synthesis of viral RNA is blocked, which stops the creation of new virions and disrupts the replication cycle within hepato-cytes[5]. Unlike other targets, NS5B remains highly conserved across various HCV genotypes, making it an excellent target for broad-spectrum antiviral drugs[6].

The development of several key inhibitors has been driven by promising therapeutic applications. These inhibitors are categorized into nucleoside inhibitors (NIs), such as Sofosbuvir[7], and non-nucleoside inhibitors (NNIs), including Dasabuvir and Beclabuvir[8]. Sofosbuvir acts as a chain terminator by being phosphorylated to its active triphosphate form, which subsequently competes with natural nucleotides for the NS5B active site[9]. The essential interactions involve hydrogen bonding with Asp225 and Ser282 residues, underscoring the importance of the phosphate group and modifications to the sugar moiety[5,10]. Conversely, NNIs bind to allosteric sites, such as the thumb or palm domains of the enzyme, inducing conformational changes that inhibit the initiation of replication[11]. While the active-site targeted NI Sofosbuvir is widely used and FDA-approved, NNIs offer a distinct mechanistic advantage by avoiding competition with high intracellular nucleotide concentrations. However, current NNIs face a critical limitation: their efficacy is highly dependent on the specific virus genotype, and they often exhibit a lower barrier to resistance compared to NIs[12]. Furthermore, many promising chemical scaffolds isolated in early-stage discovery fail in clinical trials due to poor bioavailability, high toxicity, or unfavorable pharmaco-kinetic behaviors[13]. Therefore, there is an urgent need to identify new chemical scaffolds that combine broad-spectrum pan-genotypic allosteric inhibition with optimized drug-like properties[14].

To address these dual challenges of genotype-resistance and poor drug-likeness, this study focuses on the rational design of novel quinazolinone derivatives (QD) as potential NS5B inhibitors. Quinazolinone cores represent a privileged scaffold in medicinal chemistry, known for their structural versatility and diverse pharmacological profiles. Starting with the high resolution structural data of the NS5B-QD14 complex (PDB ID: 4JJU)[15], we systematically explored *in-situ* modifications to optimize both binding affinity and safety profiles.

Traditional experimental screening of extensive chemical libraries is costly, time-consuming, and frequently overlooks pharmacokinetic flaws until late in development. To overcome this efficiency gap, our research utilized a rigorous, multi-step computational strategy designed to filter out weak candidates early. Initially, a quantitative structure-activity relationship (QSAR) model was constructed using a training set of QD with known experimental inhibitory activities[15], linking chemical structure to thermodynamics via a Molecular Mechanics Poisson-Boltzmann (MM-PBSA) approach. Subsequently, a pharmacophore (PH4) model was derived from the bound conformations of the training set molecules to map the essential chemical features required for high-affinity binding. A virtual screening was then executed using this PH4 model to rapidly assess a virtual library of analogues, ensuring that newly proposed modifications retained or enhanced critical receptor interactions. Finally, the pharmacokinetic profiles of the selected analogues were rigorously evaluated to ensure favorable ADME properties, and their structural stability within the dynamic biological environment was verified through molecular dynamics simulations.

Ultimately, this integrated methodology directly addresses the limitations of current HCV therapies by streamlining the discovery of potent, structurally stable antiviral agents that possess both high pan-genotypic target affinity and optimized pharmacokinetic properties.

MATERIALS AND METHODS

Test and validation set of quinazolinone derivatives

The QSAR model was developed using 32 quinazolinone derivatives obtained from the literature[15], with experimental inhibitory activities ranging from 60 nM to 64,000 nM. This substantial variation in activity enabled the construction of a robust QSAR model. A total of 24 quinazolinone derivatives were employed for the training and test set, while 8 were used for the validation set. Discovery Studio software[16]. was employed to partition the 32 quinazolinone derivatives into the test and validation sets.

Model construction

Three-dimensional molecular models of the NS5B-QD1-24 complexes, the NS5B polymerase, and the QD1 to QD24 inhibitors were constructed from the NS 5B-QD14 complex (PDB ID: 4JJU, resolution: 1.91 Å)[15] using Insight-II software[17] via *in situ* modification of the co-crystallized ligand QD14 (Figure 1).

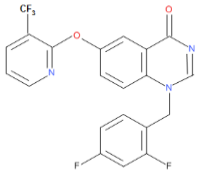

Figure 1: Initial quinazolinone derivative (QD14).

Figure 2 illustrates the principal interactions of QD14 with the nearest active site residues. To ensure the reliability of the models, each structure underwent a systematic conformational analysis combined with a stepwise energy optimization protocol. The lowest-energy states were stabilized through a global minimization of the system, following a standardized approach in the field of computer-aided drug design (CADD)[18].

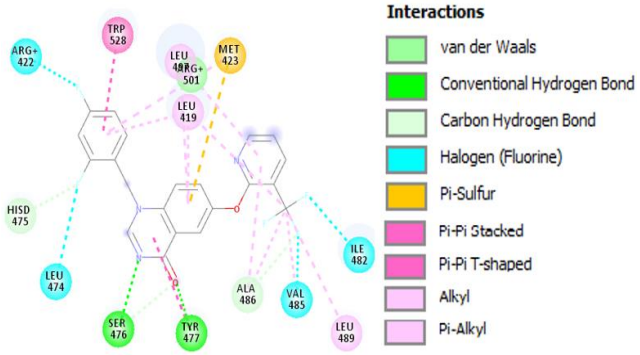

Figure 2: 2D interactions of the NS5B-QD14 complex at the active site.

These computational protocols were implemented using the Discovery Studio[16] and Insight-II[17] software suites.

Molecular mechanics

We used a detailed atomic model and the charge parameters from the CFF force field to study the QD inhibitors, the NS5B protein, and their complexes. The molecular mechanics procedures implemented were executed according to the methodology described by Frecer and co-workers[19,20].

Conformational search

The structures of the inhibitors in their unbound state were determined by relaxing their geometries from the enzyme-inhibitor complex (E: I) to the nearest local energy minimum. The conformational space was subsequently examined using the Monte Carlo method, permitting up to 50,000 iterations on all non-cyclic rotatable bonds, facilitated by the discover software[17]. For each inhibitor, 200 unique conformations were generated by applying random alterations to torsion angles by ±15° at a temperature of 5000 K, followed by energy minimization. During this process, a dielectric constant of (ε=80) was utilized to simulate the hydration related screening effect. The conformer exhibiting the lowest total energy was ultimately selected and subjected to further minimization with a constant of (ε=4).

Solvation free energy

The electrostatic component of the solvation Gibbs free energy (GFE), which includes the effects of ionic strength, was determined by solving the non-linear Poisson-Boltzmann equation[21]. This was accomplished using the Delphi module within Discovery Studio[16]. In this model, the solvent is represented as a continuous medium with high permittivity (ε=80), while the solute is considered a cavity with a low dielectric constant (ε=4). By applying finite difference methods on a cubic grid, along with physiological ionic strength and the parameters from the CFF force field, the GFE was derived as the reaction field energy[21].

Binding Energy calculation and QSAR Model

The exhaustive methodology regarding the determination of binding affinity, quantified by the Gibbs free energy (ΔG_{com}) of complexation has been previously described in detail[22]. This calculation protocol, based on the equilibrium between solvated and bound states, relies on established theoretical frameworks for the evaluation of protein-ligand interactions[23].

Interaction energy

The quantification of interaction energies within the active site was performed using the CFF force field, in accordance with established computational procedures[19]. This calculation is based on the sum-ation of non-bonding contributions, including Van der Waals potentials and electrostatic interactions[24].

Pharmacophore generation

The development of 3D-QSAR pharmacophore models was carried out using the bioactive conformations of the inhibitors extracted from the enzyme-ligand complexes. This modeling relied on the Catalyst HypoGen algorithm[25], implemented within the Discovery Studio environment (Accelrys Inc., 2009). This methodological approach follows the validation protocols described by Bieri[26].

ADME properties

To anticipate the pharmacokinetic profile of the new analogues, ADME descriptors were calculated using the QikProp program[27] following the methodology of Duffy and Jorgensen[28].

Virtual library

A virtual chemical library was constructed using the CombiLib protocol (Discovery Studio 2016) by systematically grafting R-groups onto the QD core, according to the methodology reported by Roméo[29].

ADME-based library screening

The primary virtual chemical library was subjected to rigorous filtering based on drug-likeness descriptors to select only those QD analogues exhibiting an optimal pharmacokinetic profile[30]. This molecular curation process enabled the exclusion of compounds that did not comply with established criteria for oral bioavailability and membrane permeability[31].

Pharmacophore-based library screening

The QD chemical library was refined through pharmacophore (PH4) screening within Discovery Studio. Only analogues displaying optimal alignment with the key features required for NS5B inhibition were retained[32].

Prediction of inhibitory activity

The activity of the QD analogues selected after pharmacophore screening was then predicted using the QSAR scoring function, in accordance with established structure-activity relationship protocols[33].

Molecular dynamics

The conformational stability of the QD22 ligand and its selected analogues was evaluated through 200 ns molecular dynamics simulations, as comprehensively detailed by Frecer and Miertus[34]. These simulations were conducted using the Desmond module from Schrödinger[35], utilizing the OPLS 2005 force field.

MM-GBSA binding free energy calculation

Molecular dynamics simulations of the top analogues were employed to quantify variations in binding free energy using the MM-GBSA approach. For each inhibitor studied, the enzyme-inhibitor (E-I) complex with the lowest potential energy during the 200 nanoseconds was extracted from the trajectory and subsequently subjected to energy minimization under the OPLS 2005 force field. The selection of this force field is justified by its established accuracy in evaluating solvation energies and structural parameters of heterocyclic ligands[36]. The variation in binding free energy is formalized by the following equation:

$$\Delta G_{bind} = \Delta E_{MM} + \Delta G_{solv} + \Delta G_{SA} \quad \text{....(Eq 1)}$$

Where ΔE_{MM} is the variation in molecular mechanics energy ΔG_{solv} is the solvation energy variation, and (ΔG_{SA}) is the surface area contribution.

Statistical analysis

The QSAR model was constructed and rigorously validated using QSARINS software version 2.2.4-2019, which specifically implements the validation protocols required by the OECD (Organization for Economic Cooperation and Development)[37-43].

A univariate linear regression was established using the relative binding free energy ΔG_{bind} as the descriptor to predict the experimental biological activity as the response. The dataset (n=32) was split into a training set (n=24) and a validation set (n=8).To ensure the model's robustness, internal consistency, and external predictivity, several statistical metrics were calculated across multiple dimensions of validation. Internal robustness was evaluated using the coefficient of determination, Leave-One-Out Cross-Validation (LOO CV), and Leave-Many-Out cross-validation (LMOCV), while potential over-fitting was monitored by comparing the Root Mean Square Error and Mean Absolute Error (MAE) against their cross-validated counterparts. External predictivity was simultaneously assessed using a validation set to determine the external squared correlation coefficient, the Root Mean Square Error of the validation set ($RMSE_{ext}$) and the Mean Absolute Error of the validation set (MSE_{ext}). Finally, to confirm that the observed correlation was not due to chance, a Y-randomization test was performed over 2000 iterations of Y-scrambling, utilizing the resulting random values and the parameter which adjusts the original based on the randomization results to confirm the model's true statistical significance.

RESULTS AND DISCUSSION

Training and validation set

The training and validation set were constructed from thirty-two NS5B inhibitors (Table 1), designated as QD1–32, and sourced from benchmark studies[15]. The structural diversity and the heterogeneity of biological activities within this series ensure the robustness and predictive capacity of the developed QSAR model[44]. Using the Discovery Studio environment[16], the 32 compounds were partitioned into a training set of 24 molecules and a validation set of 8 molecules.

Table 1: Training and validation set alongside their biological activities.

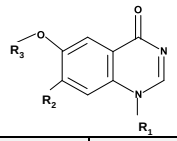

Training Set					Training Set				
Ligand	R_1	R_2	R_3	IC_{50}^{exp}(nM)	Ligand	R_1	R_2	R_3	IC_{50}^{exp}(nM)
QD1	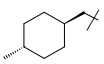	H		6900	QD13		H		200
QD2	CH_3	H		24000	QD14	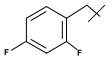	H		510
QD3		H		4300	QD15	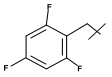	H		100
QD4	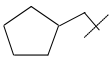	H		2400	QD16	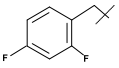	OMe		2400
QD5		H		1600	QD17	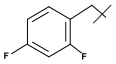	H	OMe	64000
QD6	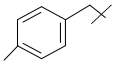	H		450	QD18	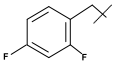	H		1200
QD7	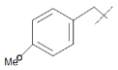	H		48000	QD19	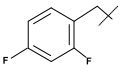	H		490
QD8	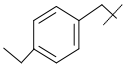	H		1100	QD20	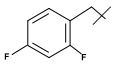	H		230
QD9	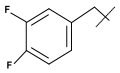	H		4000	QD21	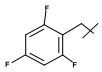	H		110
QD10	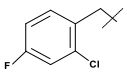	H		800	QD22	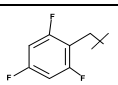	H		60
QD11	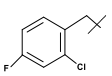	H		400	QD23		H		75
QD12		H		260	QD24		H		300

Validation set									
QD25	H	H		4400	QD29	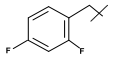	F		240
QD26	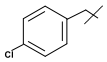	H		1100	QD30	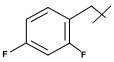	NMe_2		25000
QD27	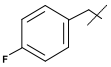	H		1200	QD31	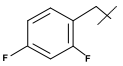	H		860
QD28	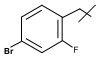	H		310	QD32	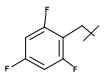	H		100

Table 2: Variation of complexation enthalpy relative to the reference ligand QD14 and its components for the training set (TS) and the validation set (VS).

TS *	M_W [a] [g.mol^{-1}]	$\Delta\Delta H_{MM}$ [b] [kcal.mol^{-1}]	$\Delta\Delta G_{solv}$ [c] [kcal.mol^{-1}]	$T\Delta\Delta S_{vib}$ [d] [kcal.mol^{-1}]	$\Delta\Delta G_{com}$ [e] [kcal.mol^{-1}]	pIC_{50}^{exp} [f]
QD1	417.16	10.82	1.71	6.78	5.76	5.16
QD2	321.07	14.44	-1.68	4.00	8.76	4.62
QD3	403.15	10.77	1.65	7.74	4.67	5.37
QD4	389.16	6.79	1.93	5.41	3.30	5.62
QD5	397,10	3.81	0.83	2.32	2.33	5.8
QD6	411.12	0.71	1.62	1.86	0.47	6.35
QD7	427.11	9.73	-0.17	0.73	8.83	4.32
QD8	425.14	2.27	3.26	3.04	2.49	5.96
QD9	433.08	0.98	1.19	-0.44	2.62	5.40
QD10	449.06	3.06	0.19	-0.52	3.77	6.10
QD11	449.06	0.12	0.86	-0.53	1.51	6.40
QD12	429.11	-3.28	3.39	0.96	-0.85	6.59
QD13	433.08	-0.59	1.25	0.37	0.29	6.70
QD14	433.08	0.00	0.00	0.00	0.00	6.29
QD15	451.08	-3.87	0.36	-0.86	-2.64	7.00
QD16	463.10	3.00	1.16	0.30	3.86	5.62
QD17	302.09	13.95	0.88	4.04	10.79	4.19
QD18	433.08	-2.05	0.21	1.73	-3.57	6.92
QD19	433.08	-2.50	0.76	1.04	-2.78	6.31
QD20	463.10	-3.17	1.43	-1.16	-0.58	6.64
QD21	451.08	-5.47	0.65	-0.29	-4.54	6.96
QD22	451.08	-5.79	1.03	0.87	-5.63	7.22
QD23	450.08	-5.98	0.56	1.03	-6.46	7.12
QD24	382.09	-0.80	0.80	3.85	-3.85	6.52
VS *	M_W [a] [g.mol^{-1}]	$\Delta\Delta H_{MM}$ [b] [kcal.mol^{-1}]	$\Delta\Delta G_{solv}$ [c] [kcal.mol^{-1}]	$T\Delta\Delta S_{vib}$ [d] [kcal.mol^{-1}]	$\Delta\Delta G_{com}$ [e] [kcal.mol^{-1}]	pIC_{50}^{exp} [f]
QD25	307.06	12.59	0.43	4.88	8.14	5.36
QD26	431.06	-0.25	0.83	0.57	0.01	5.96
QD27	415.09	0.29	0.45	1.18	-0.45	5.92
QD28	493.00	-3.74	2.89	-1.12	0.27	6.51
QD29	451.08	-1.08	0.02	-1.30	0.24	6.62
QD30	476.13	15.20	-1.68	2.55	10.97	4.60
QD31	443.01	5,10	-0,15	2,73	2,23	6.07
QD32	481.09	-6,87	1,01	-1,97	-3,89	7.00

*For the chemical structures of training set, validation set, and IC_{50}^{exp} see (Table 1) ; [a]M_W is the molar mass of inhibitors ;[b]$\Delta\Delta H_{MM}$ is the relative enthalpic contribution to the GFE change related to E:I complex formation derived by MM : $\Delta\Delta H_{MM} \cong [E_{MM}\{E:I_x\} - E_{MM}\{I_x\}] - [E_{MM}\{E:I_{ref}\} - E_{MM}\{I_{ref}\}]$. I_{ref} is the reference inhibitor QD14 ; [c]$\Delta\Delta G_{sol}$ is the relative solvation Gibbs free energy contribution to the Gibbs free energy related to E:I complex formation : $\Delta\Delta G_{sol} = [G_{sol}\{E:I_x\} - G_{sol}\{I_x\}] - [G_{sol}\{E:I_{ref}\} - G_{sol}\{I_{ref}\}]$; [d]$\Delta\Delta TS_{vib}$ is the relative entropic contribution of the inhibitor to Gibbs free energy to E:I complex formation : $\Delta\Delta TS_{vib} = [\Delta\Delta TS_{vib}\{I_x\}_E - \Delta\Delta TS_{vib}\{I_x\}] - [\Delta\Delta TS_{vib}\{I_{ref}\}_E - \Delta\Delta TS_{vib}\{I_{ref}\}]$;[e]$\Delta\Delta G_{com}$ is the relative Gibbs free energy to E:I complex formation : $\Delta\Delta G_{com} \cong \Delta\Delta H_{MM} + \Delta\Delta G_{sol} - \Delta\Delta TS_{vib}$; [f]$pIC_{50}^{exp} = -log_{10}(IC_{50}^{exp})$.

This balanced distribution guarantees an optimal coverage of the chemical space and activity ranges for both model calibration and external validation[44].

QSAR Model

Single-descriptor QSAR

The relative Gibbs free energy was calculated for each NS5B-QDx complex based on the crystal structure of NS5B (PDB ID: 4JJU)[45]. Table 2 summarizes the calculated values of as well as its various components for both the training and validation set.

A Hansch-type QSAR model was developed by creating a linear regression (Figure 3) that linked the experimental activities with the values. This model explains approximately 90% of the variance in experimental activities (Table 3).

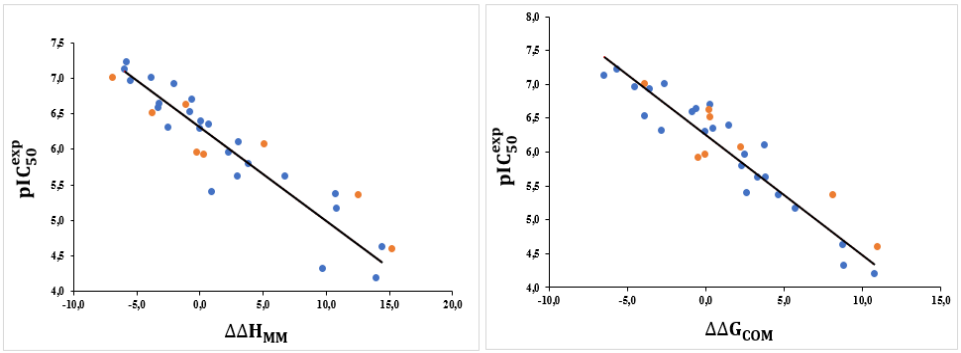

Figure 3: (Left) plot of correlation (Table 3) between pIC_{50}^{exp} and $\Delta\Delta H_{MM}$ [kcal. mol^{-1}]. (Right) plot of the rGFE of the NS5B-QDx complex formation $\Delta\Delta G_{com}$ [kcal. mol^{-1}].

The dots from validation set are shown in orange.

Table 3: Regression analysis of $\Delta\Delta G_{com}$. its enthalpic component $\Delta\Delta H_{MM}$ and experimental activity $pIC_{50}^{exp} = -\log_{10}(IC_{50}^{exp})$ of QD toward NS5B.

	$pIC_{50}^{exp} = -0.1316 * \Delta\Delta H_{MM} + 6.3065$ (Eq 2)	$pIC_{50}^{exp} = -0.1779 * \Delta\Delta G_{com} + 6.2608$ (Eq 2)
N	24	
IC_{50}^{exp}range	60 nM – 64000 nM	
Internal validation		
R^2	0.87	0.90
σ	0.31	0.28
Fischer F-Test	153.43	199.11
α	95%	95%
RMSE	0.30	0.27
MAE	0.23	0.21
R^2_{LOOCV}	0.85	0.88
R^2_{LMOCV}	0.84	0.88
$RMSE_{CV}$	0.33	0.29
MAE_{CV}	0.25	0.23
External validation		
R^2_{ext}	0.59	0.69
$RMSE_{ext}$	0.62	0.46
MAE_{exT}	0.52	0.41
Y-Randomization for 2000 iterations of shuffling		
R^2_{YSCT}	0.04	0.04
R^2_P	0.80	0.83

N: Number of compounds; R^2: Coefficient of determination; RMSE: Root mean square error, MAE: Mean absolute error; R^2_{LOOCV} : Leave-one-out cross-validation (LOOCV) coefficient of determination; σ: Standard error of regression; α: Level of statistical significance; R^2_{LMOCV} :Leave-more-out cross-validation (LMOCV) coefficient of determination.

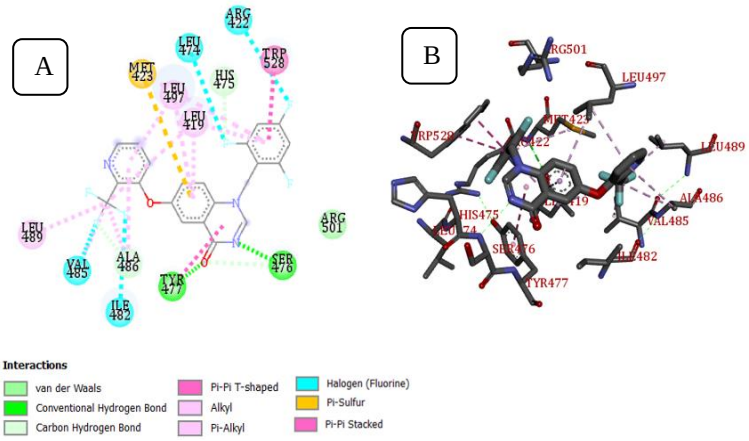

Figure 4: A: 2D interactions diagram of the most potent inhibitor (QD22) at the NS5B active site (from the native crystal structure). B: 3D interactions pattern of QD22 at the NS5B active site (from QSAR model).

The statistical robustness of this correlation is confirmed by high R^2 and R^2_{XV} values, as well as a significant Fisher test (F=199.11, (Table 3). Furthermore, the gas-phase enthalpy was correlated with the pIC_{50}^{exp} values (Table 3). This correlation highlights the predominant contribution of interatomic interactions, which alone account for about 87% of the variation in biological activity.

Table 4: Statistical parameters of the 10 PH4 pharmacophore hypotheses generated for NS5B inhibitors after the "Cat-Scramble" validation procedure (Accelrys Inc., 2009) (49 randomization trials for each hypothesis at the selected 98% confidence level).

Hypothesis	RMSD[a]	R^2 [b]	Total costs[c]	Cost difference[d]	Closet random[e]
Hypo 1	3.17	0.90	178.77	525.13	406.71
Hypo 2	3.41	0.88	197.18	506.71	427.10
Hypo 3	3.41	0.88	197.89	506.01	445.08
Hypo 4	3.42	0.88	199.59	504.31	452.71
Hypo 5	3.46	0.88	203.28	500.61	456.65
Hypo 6	3.49	0.88	204.02	499.88	457.96
Hypo 7	3.50	0.88	206.22	497.67	458.24
Hypo 8	3.61	0.87	215.21	488.69	463.93
Hypo 9	3.68	0.86	221.77	482.12	476.69
Hypo 10	3.70	0.86	222.48	481.42	479.96

[a]root means square deviation; [b] squared correlation coefficient; [c] overall cost parameter of the PH4 pharmacophore; [d] cost difference between Null cost and hypothesis total cost; [e] lowest cost from 49 scrambled runs at a selected confidence level of 98%. The Fixed Cost = 57.20 with RMSD = 0, the Null Cost = 703.9 with RMSD = 7.40 and the Configuration cost = 9.72.

Utilizing QSARINS software, we calculate additional key statistical parameters as detailed in Table 3, in compliance with OECD guidelines for regulatory QSAR models[38,39,43]. The QSAR model, can handle up to 30% of perturbation without affecting the LOOCV R^2_{XV} (0.88) and LMOCV Q^2_{XV} (0.88) values. Furthermore, the Y-scrambling method, which involves the random shuffling of responses, results in a low average R^2Yscr value (0.04), markedly lower than the original model's value (0.90), indicating that the model is not subject to random correlations. Additionally, the model's predictive capability is assessed through low RMSE values for the training set (RMSE, 0.27), the cross-validation ($RMSE_{CV}$, 0.29), and the validation set ($RMSE_{ext}$, 0.46). The proximity of these RMSE values suggests enhanced generalizability of the model.

In conclusion, this QSAR model is statistically rigorous and perfectly suited for predicting the affinity of new QD analogues sharing a comparable binding mode.

Molecular interaction analysis and binding mode

Examination of the NS5B–QD22 complex, modeled from the reference crystallographic structure (PDB ID: 4JJU)[15], highlights a synergistic binding mode. The stability of the complex is primarily governed by a network of robust hydrogen bonds (His 475, Ser 476, Tyr 477) and π-π stacking interactions (Tyr 477, Trp 528), which ensure a rigid anchoring of the scaffold (Figure 4). Furthermore, the strong shape complementarity observed with the residues (Leu 419, Leu 497, Leu 489, Ala 486, and Val 485) of the polymerase's hydrophobic pocket via π-alkyl interactions[45] minimizes the Gibbs free energy, conferring a high predictive affinity to the QDx series. These interactions confirm that the QDx compounds optimally occupy the binding site, thereby effectively blocking the enzymatic activity of NS5B.

3D-QSAR pharmacophore model

A 3D-QSAR pharmacophore model for NS5B inhibition was designed using the bound conformations of all molecules from the training set and subsequently validated using the ligands from the validation set. This construction was performed as described in references[26,46]. To maximize the accuracy of the model and enhance its robustness, the biological activity uncertainty was reduced to 1.1. Among the ten best generated pharmacophores, the optimal model was selected (Table 4). It is characterized by a maximum cost difference (525.13), the highest correlation coefficient (0.86), the lowest RMSD value (3.17), and an acceptable configuration cost (9.62)[16].

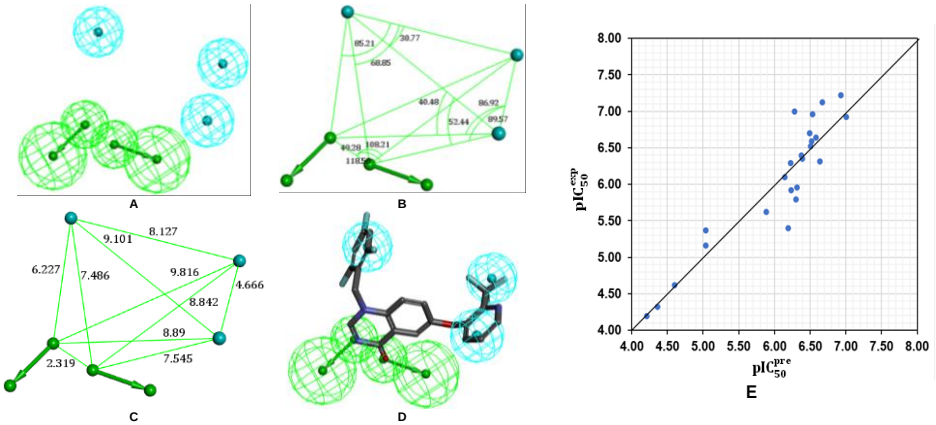

Figure 5: The optimal pharmacophore model (Hypo1) of NS5B inhibition: (A) feature, (B) distances (Å) between features, (C Angles (°) between centers of pharmacophoric features, (D) Mapping of QD22 to the pharmacophore. Features color legend: Hydrophobic (cyan), Hydrogen bond Acceptor Projection (green). (E) Correlation plot of experimental *vs* predicted inhibitory activity.

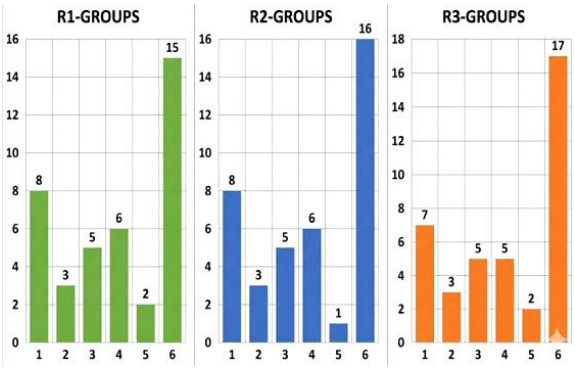

Figure 6: Frequency of occurrence histogram of Ri clusters among the best quinazolinone analogues derived from the PH4 pharmacophore screening of the generated virtual chemical library.

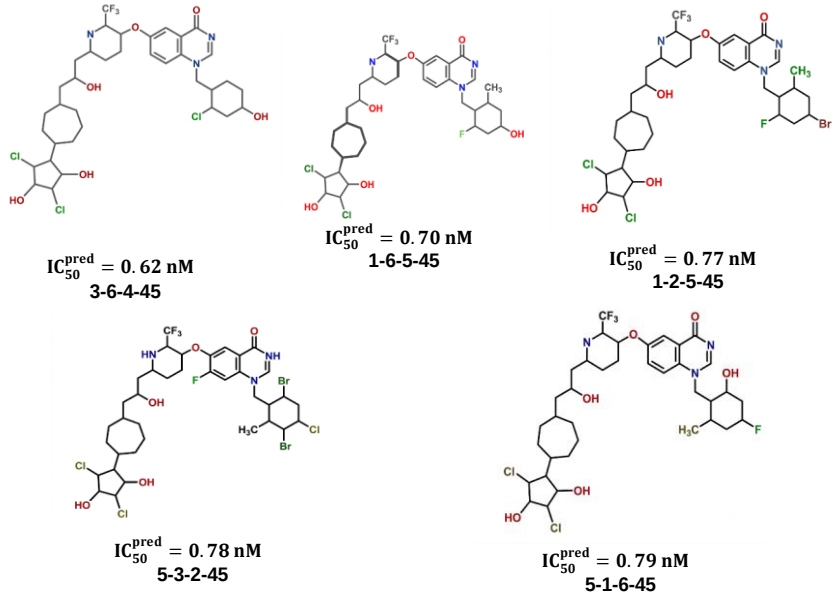

$IC_{50}^{pred} = 0.62$ nM
3-6-4-45

$IC_{50}^{pred} = 0.70$ nM
1-6-5-45

$IC_{50}^{pred} = 0.77$ nM
1-2-5-45

$IC_{50}^{pred} = 0.78$ nM
5-3-2-45

$IC_{50}^{pred} = 0.79$ nM
5-1-6-45

Figure 7: The most effective QD analogues with a scaffold of NS5B are designated $\#R_1$-$\#R_2$-$\#R_3$-$\#R_4$.

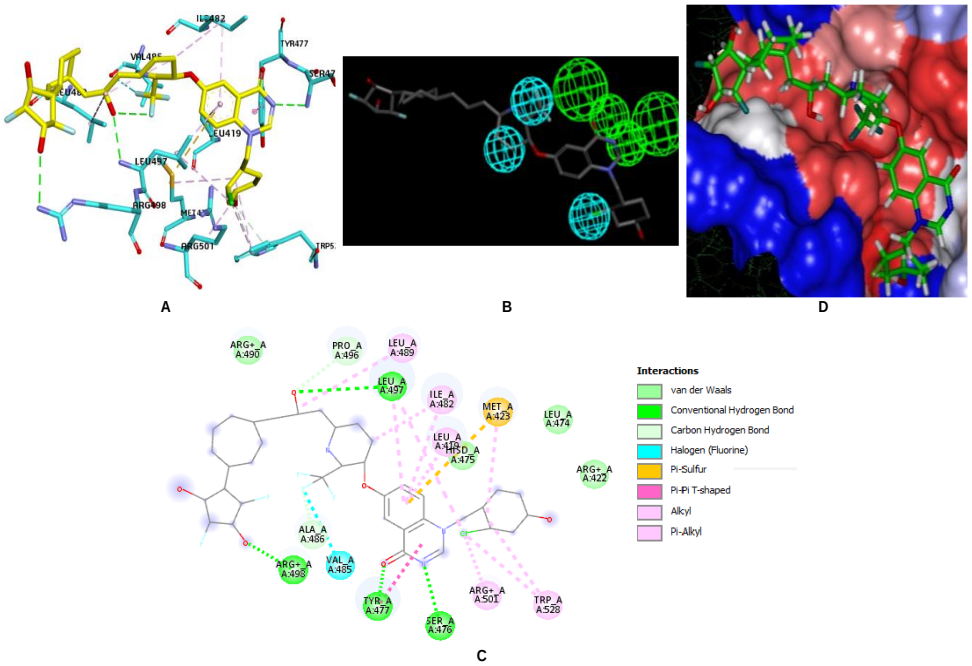

Figure 8: (A): 3D interactions pattern of 3-6-4-45 ($IC_{50}^{pred} = 0.62$ nM, the most active designed QD analogue) and the active site residues of NS5B; (B): Mapping of the 3-6-4-45 to NS5B inhibition pharmacophore. (C): 2D schematic interaction diagram of 3-6-4-45. (D): Connolly surface of the active site of NS5B (the binding site surface was colored according to residue hydrophobicity: red = hydrophobic, blue = hydrophilic and white = intermediate).

Table 5: R1, R2, R3 and R4-groups (fragments, building blocks, substituents) used in the design of the initial virtual combinatorial library of QD analogues.

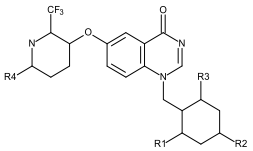

R-groups*					
1	Fluoro	2	Bromo	3	Chloro
4	Hydrogen	5	Methyl	6	Hydroxy
7	Methoxy	8	Amonia	9	Methanol
10	Fluoroform	11	Formic acid	12	methylsulfonyl
13	Isopropyl	14	Propyl	15	Cyclopropyl
16	3-(3-iodopropyl)cyclohexanol	17	5-pentylpiperidin-2-ol	18	5-amino-2-pentyl-cyclohexane-1,3-diol
19	4-butylcyclohexanamine	20	3-pentylcyclohexanamine	21	4-amino-3-pentyl-cyclohexanol
22	(4-pentylcyclohexyl) hydroxylamine	23	[3-pentylcyclohexyl]hydroxylamine	24	[2-pentylcyclohexyl]hydroxylamine
25	2-amino-5-pentyl-cyclohexanol	26	2-amino-4-pentyl-cyclohexanol	27	3-amino-2-pentyl-cyclohexanol
28	4-amino-3-pentyl-cyclohexanol	29	3-amino-4-pentyl-cyclohexanol	30	O-[3-pentylcyclohexyl] hydroxylamine
31	O-(4-pentylcyclohexyl) hydroxylamine	32	O-[2-pentylcyclohexyl] hydroxylamine	33	2-hydroxy-4-pentyl-cyclohexanecarboxamide
34	3-hydroxy-4-pentyl-cyclohexanecarboxamide	35	4-pentylcyclohexanecarboxylic acid	36	4-(4-pentylcyclohexyl) cyclohexanecarboxamide
37	4-(4-butylcyclohexyl)cyclohexanecarboxylic acid	38	7-butyldecalin-2-carboxamide	39	7-butyldecalin-2-carboxamide
40	methyl 4-(4-pentylcyclohexyl) cyclohexanecarboxylate	41	trifluoromethyl 4-(4-butylcyclohexyl)cyclohexane-carboxylate	42	4-aminooxy-7-pentyl-adamantan-2-ol
43	4-[2-[6-(2-cyclohexylethyl)-3-piperidyl]ethyl]-cyclohexanecarboxamide	44	6-[2-[4-(2-cyclohexylethyl) cyclohexyl] ethyl]piperidine-3-carboxylic acid	45	2,4-difluoro-5-[4-butylcyclo-heptyl]cyclopentane-1,3-diol
45	2,4-difluoro-5-[4-butylcyclo-heptyl]cyclopentane-1,3-diol	46	2,3,5,6-tetrafluoro-N-(hydroxymethyl)-4-[3-[1,3-dimethylbutyl]cyclobutyl] cyclohexanecarboxamide	47	2-[3-pentylcyclohexyl]acetamide
48	2-[3-pentylcyclohexyl]-N-[1,2,3-trifluorocyclopropyl]acetamide	49	2-[3-butylcyclohexyl]-N-[2-chloro-1,3-difluoro-cyclopropyl]acetamide	50	2-[3-butylcyclohexyl]-N-[1,2-difluoro-3-sulfanyl-cyclopropyl]acetamide
51	2-amino-3-(4-butylcyclohexyl)propanal	52	2-amino-3-methyl-4-[3,5-dihydroxy-4-pentyl-cyclohexyl]butanal	53	2-amino-5-(4-butylcyclohexyl)-4-methyl-pentanal
54	4-(4-pentylcyclohexyl) pyrrolidine-2-carbaldehyde	55	4-(4-butylcyclohexyl)-2-(trifluoro methyl)pyrrolidine-2-carbaldehyde	56	4-(4-butylcyclohexyl)-2-fluoro-pyrrolidine-2-carbaldehyde
57	2-chloro-4-(4-pentylcyclohexyl) pyrrolidine-2-carbaldehyde	58	2-bromo-4-(4-pentylcyclohexyl) pyrrolidine-2-carbaldehyde	59	2-hydroxy-4-(4-pentylcyclohexyl) pyrrolidine-2-carbaldehyde
60	4-(4-butylcyclohexyl)-2-sulfanyl-pyrrolidine-2-carbaldehyde	61	2-[4-[3-cyclopropylbutyl] cyclohexyl]cycloheptane-1,3,5-triol	62	2-amino-3-[4-[4-[3-cyclopropyl butyl]cyclohexyl]cycloheptyl]propanal
63	2-amino-3-methyl-4-[4-[4-[3-cyclopropylbutyl]cyclohexyl]cycloheptyl]butanal	64	2-amino-4-methyl-5-[4-[4-[3-cyclopro pylpentyl] cyclohexyl]cycloheptyl]pentanal	65	4-[4-[4-[3-cyclopropylpentyl] cyclohexyl]cycloheptyl]pyrrolidine-2-carbaldehyde

R1: 1→15; R2: 1→15; R3: 1→15; R4: 16→65

Linear regression analysis confirms the predictive accuracy of the selected model, displaying a slope close to unity (1.024) and a y-intercept close to zero (0.1419)[42]. The regression equation and its associated statistical parameters are as follows:

$pIC_{50}^{exp} = 1.0058 \times pIC_{50}^{pre} + 0.0353$; n=32, $R^2=0.85$

$R^2_{XV} = 0.84$, F-test=130.30; σ=0.34, α=95%

The correlation plot is illustrated in Figure 5E. Furthermore, the proper alignment of molecule QD22 with the pharmacophoric features of the PH4 model is shown in Figure 5D. Ultimately, this final PH4 model served as a predictive tool for pIC_{50} during the screening of a chemical library of QD analogues.

Virtual screening

The *in silico* screening of virtual combinatorial chemical libraries represents a choice strategy for identifying lead compounds (hits), as demonstrated by the work of Bléhoué *et al.*[33].

Virtual library

A preliminary virtual library was constructed by systematically diversifying the quinazolinone (QD) scaffold at positions R1, R2, R3, and R4 (Table 5). The combinatorial introduction of 15 distinct substituents at each of the first three sites, and 50 substituents at the final site (R4), generated a chemical space of 168,750 structural analogues. All of these derivatives strictly

maintain the substitution pattern of the most active reference inhibitor to preserve key interactions.

To optimize the drug-like profile of the molecules, a series of selection filters was applied. This protocol integrates Lipinski's "rule of five", limiting molecular weight to 500 g/mol to ensure good oral bio-availability[48]. In the framework of this study, this filter was readjusted to also encompass the criteria required for potential intravenous administration. This rigorous filtration phase yielded a targeted, pharmacologically relevant chemical library optimized for subsequent virtual screening steps.

Virtual library screening

This library of 168,750 analogues was subjected to an *in-silico* evaluation to isolate molecular structures matching the geometric and electronic features of the 3D-PH4 Hypo1 pharmacophore model (NS5B inhibition). Following this filtering process, a total of 200 QD analogues satisfied the required pharma-cophoric characteristics. These preselected compounds (PH4 hits) were subsequently evaluated using the QSAR complexation model. The Gibbs free energy of NS5B-QD complex formation, its various energetic components, and the predicted values of the negative logarithm of the half-maximal inhibitory concentration (Table 6).

Substituent analysis of new QD analogues

In order to highlight the key substituents responsible for enhanced NS5B inhibition, an analysis was conducted on the 200 virtual hits aligned with the PH4 pharmacophore. Evaluation of the substituent distribution frequency at positions R_1, R_2 and R_3 (Figure 6) indicates that the introduction of small fragments at R_1, R_2 and R_3 favors inhibitory activity, whereas at R_4 activity is improved with the addition of bulky substituents. Notably, analogue 3-6-4-45 (Figure 7 and Figure 8) displays a predicted activity approximately 96-fold higher than that of the reference compound[45].

Table 6: Top 15 most active analogues and their predicted semi-maximal inhibitory concentrations.

	Analogues	M_w[a] [g.mol^{-1}]	$\Delta\Delta H_{MM}$[b] [kcal.mol^{-1}]	$\Delta\Delta G_{sol}$[c] [kcal.mol^{-1}]	$T\Delta\Delta S_{vib}$[d] [kcal.mol^{-1}]	$\Delta\Delta G_{com}$[e] [kcal.mol^{-1}]	IC_{50}^{pre}[f] [nM]
Ref	QD22 *	451,08	0.00	0.00	0.00	0.00	60
1	1-2-5-45	809.28	4.35	5.12	25.69	-16.22	0.77
2	1-2-6-45	811.26	2.95	8.02	24.92	-13.96	1.95
3	1-3-4-45	751.32	4.76	5.39	24.62	-14.48	1.57
4	1-4-6-45	733.35	3.98	6.67	25.43	-14.78	1.39
5	1-6-3-45	767.31	7.59	4.94	26.77	-14.25	1.73
6	1-6-5-45	747.37	6.27	4.57	27.30	-16.46	0.70
7	2-1-6-45	811.26	2.70	6.85	24.96	-15.41	1.08
8	2-6-4-45	793.27	5.89	6.67	26.40	-13.85	2.04
9	3-6-4-45	749.32	6.04	4.71	27.50	-16.75	0.62
10	5-1-6-45	747.37	3.73	5.66	25.55	-16.17	0.79
11	5-3-2-45	825.25	-0.32	4.18	20.06	-16.20	0.78
12	5-6-1-45	747.37	4.72	6.05	24.07	-13.30	2.54
13	6-3-3-45	783.28	3.47	5.95	23.24	-13.82	2.06
14	6-3-4-45	749.32	6.58	5.74	25.19	-12.87	3.03
15	4-1-3-45	751.32	4.49	3.95	24.78	-16.35	0.74

[a]M_w is the molar mass of inhibitors ; [b]$\Delta\Delta H_{MM}$ is the relative enthalpic contribution to the GFE change of the NS5B-QD complex formation $\Delta\Delta G_{com;}$ [c] is the relative solvation GFE contribution to $\Delta\Delta G_{com}$; [d]$T\Delta\Delta S_{vib}$ is the relative (vibrational) entropic contribution to$\Delta\Delta G_{com}$; [e]$\Delta\Delta G_{com}$ is the relative Gibbs free energy change related to the enzyme-inhibitor NS5B-QD complex formation : ; [f] IC_{50}^{pre} is the predicted inhibition potency towards NS5B calculated from $\Delta\Delta G_{com}$ using Table 3; IC_{50}^{pre} given for the most active inhibitor QD1 instead of the IC_{50}^{pre} .

Molecular dynamics

To evaluate the structural stability of the studied complexes, 200ns molecular dynamics simulations were performed for the most active ligand from the training set (QD22) and the top six analogues (1-2-5-45, 1-6-5-45, 4-1-3-45, 3-6-4-45, 5-1-6-45, and 5-3-2-45) [49]. Examination of the root-mean-square deviations (RMSD) highlights good structural convergence (Figure 9, Figure 11). The reference complex (QD22) maintains an RMSD below 1.2 Å throughout the trajectory, while the analogues exhibit variations between 1.5 Å and 3 Å. These values ($1.5 \leq RMSD \leq 3$ Å) demonstrate that the introduced structural modifications do not affect the conformational equilibrium of the systems, as explained by Rana and co-workers[50].

The time evolution of the radius of gyration (rGyr) served as an indicator of compactness. The (system/ complex) maintains an invariant value at 4.40 Å, reflecting high rigidity and dynamic stability.

The analogues display rGyr values converging between 6.4 and 8.8 Å. These results show a displacement of the protein backbone (increasing the size of the pocket) according to Olivier Hucke and associates[51], causing binding of the analogues with residues Pro 496, Leu 497, and Arg 498. This movement improves activity through hydrogen bonds and carbon-hydrogen bonds established with residues Arg 498, Leu 497, and Pro 496.

Binding mode and interaction energy of new inhibitors

Analysis of the interaction diagram (Figures 10 and 12) illustrates the stable anchoring of the most active analogue within the allosteric pocket 2 of the NS5B polymerase. The oxoquinoline core forms key hydro-gen bonds with Tyr477 and Ser476, as described in the work of marina[52], which are further reinforced by a π-sulfur interaction with Met423, thereby blocking the transition of the polymerase toward its active form[53].

Table 7: ADME properties of the designed lead QD analogues and known Hepatitis C drugs currently in clinical use, computed by QikProp (Schrödinger, 2019).

Compounds	#Stars[b]	M_w[c] g.mol^{-1}	S_{mol}[d] (A^2)	$S_{mol.hfo}$[e] (A^2)	V_{mol}[f] (A^3)	RotB[g]	HB_{don}[h]	HB_{acc}[i]	$logP_{o/w}$[j]	$logS_{wat}$[k]	$logK_{HSA}$[l]	logB/B[m]	BIP_{caco}[n] nm.S^{-1}	#meta[o]	IC_{50}^{pre}[p] (nM)	HOA[q]	%HOA[r]
3-6-4-45	8	750.3	1051.6	518.4	2050.9	12	5	12.5	4.8	-7.9*	0.9	-2.3	9.3	5	0.62	1	59.5
1-6-5-45	8	747.8	1072	545.6	2083.3	12	5	12.5	4.8	-8.1*	1	-2.5	8.2	5	0.70	1	58.8
1-2-5-45	11	810.7	1099.6	558.8	2124.3	11	4	10.8	6.6	-9.7*	1.5	-1.7	26.2	4	0.77	1	65.1
5-3-2-45	11	827.2	1098.8	527.7	2135.8	11	4	10.8	6.7	-9.8*	1	-1.6	24.3	4	0.78	1	65.4
5-1-6-45	9	747.8	1065.7	549.4	2093.3	12	5	12.5	5.1	-8.1*	1	-2.1	13.6	5	0.79	1	51.6
Sofosbuvir	0	529.5	755.4	356.2	1460.8	10	3	14.9	0.9	-3.4	-0.6	-2.1	76.1	4		2	40.1
Dasabuvir	1	493.6	786.8	295.4	1456.4	5	2	8.7	3.3	-6.5*	-0.6	-2.2	59.7	2		1	78.2
Ombitasvir	13	894.1	1472.8	1037.8	2828.7	11	2,5	15.5	8.1	-13.4*	1.8	-2.7	113.2	7		1	72.1
Ledipasvir	11	889.0	1363.8	775,4	2628.9	7	2,5	12.5	8.5	-136*	2.1	-2.2	95.4	4		1	73.1
Velpatasvir	12	883.0	1375.1	735,9	2633.9	8	2,5	14.9	7.3	-12.6*	1.5	-2.5	118.6	7		1	68
Pibrentasvir	15	1113.2	1608.1	972,4	3142.5	8	2,5	17.9	9.6	-15.6*	2.2	-2.4	73.4	10		1	77.4

[a] designed QD analogues and known anticancer agents, Table 6; [b] drug likeness, number of property descriptors (24 out of the full list of 49 descriptors of QikProp, ver. 3.7, release 14) that fall outside of the range of values for 95% of known drugs; [c] molecular weight (range for 95% of drugs: 130-725 g.mol^{-1} [X]; [d] total solvent-accessible molecular surface, (probe radius 1.4 Å) (range for 95% of drugs: 300 – 1000 Å^2); [e] hydrophobic portion of the solvent-accessible molecular surface (probe radius 1.4 Å) (range for 95% of drugs: 0 – 750 Å^2); [f] total volume of molecule enclosed by solvent-accessible molecular surface, (probe radius 1.4 Å) (range for 95% of drugs: 500 - 2000 Å^3); [g] number of non-trivial (not CX3), non-hindered (not alkene, amide, small ring) rotatable bonds (range for 95% of drugs: 0 - 15); [h] estimated number of hydrogen bonds that would be donated by the solute to water molecules in an aqueous solution. Values are averages taken over several configurations, so they can assume non-integer values (range for 95% of drugs: 0.0 - 6.0); [i] estimated number of hydrogen bonds that would be accepted by the solute from water molecules in an aqueous solution. Values are averages taken over several configurations, so they can assume non-integer values (range for 95% of drugs: 2.0 - 20.0); [j] logarithm of partitioning coefficient between n-octanol and water phases (range for 95% of drugs: -2 - 6.5); [k] logarithm of predicted aqueous solubility, logS in (mol.dm^{-3}) is the concentration of the solute in a saturated solution that is in equilibrium with the crystalline solid (range for 95% of drugs: -6.0 - 0.5); [l] logarithm of predicted binding constant to human serum albumin (range for 95% of drugs: -1.5 - 1.5); [m] logarithm of predicted brain/blood partition coefficient (range for 95% of drugs: -3.0 - 1.2); [n] predicted apparent Caco-2 cell membrane permeability in Boehringer-Ingelheim scale (range for 95% of drugs: < 25 poor, > 500 nm s^{-1} great); [o] number of likely metabolic reactions (range for 95% of drugs: 1–8); [p] predicted inhibition constants IC_{50}^{pre} was predicted from computed $\Delta\Delta G_{com}$; [q] human oral absorption (1 = low, 2 = medium, 3 = high); [r] percentage of human oral absorption in gastrointestinal tract (<25% = poor, >80% = high); * star in any column indicates that the property descriptor value of the compound falls outside the range of values for 95% of known drugs.

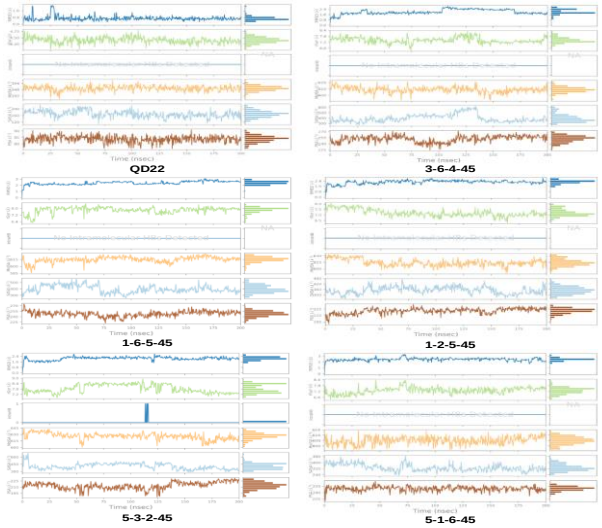

Figure 9: Time-evolution of the properties of the NS5B-QDx complexes during 200 ns MD simulation.

For each inhibitor, top to bottom: plot of the root mean square deviation (RMSD) with respect to the initial conformation vs. The simulation time, radius of gyration (rGyr), number of intramolecular hydrogen bonds (intraHB), molecular surface area (molSA), solvent-accessible surface area (SASA), and polar surface area (PSA).

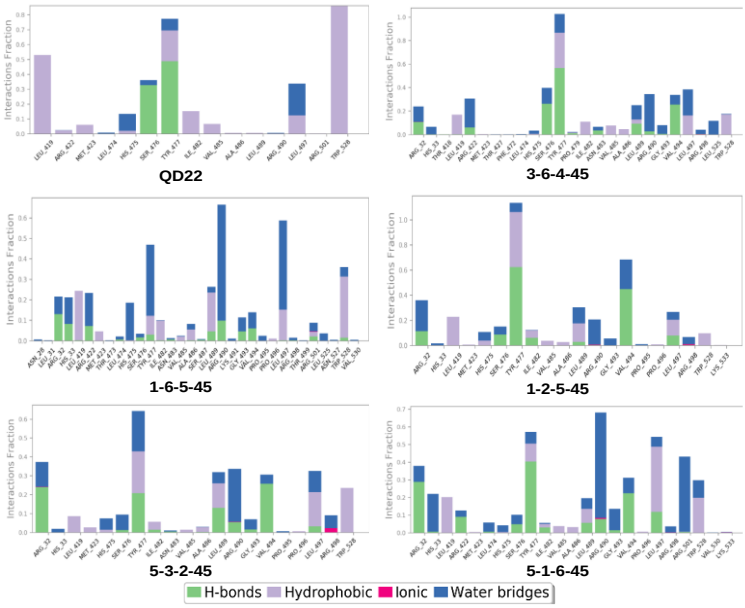

Figure 10: Contribution of individual active site residues to inhibitor binding in NS5B-QDx complexes present during MD simulations: HB (green); ionic interactions (magenta); hydrophobic contacts (purple); water bridges (blue).

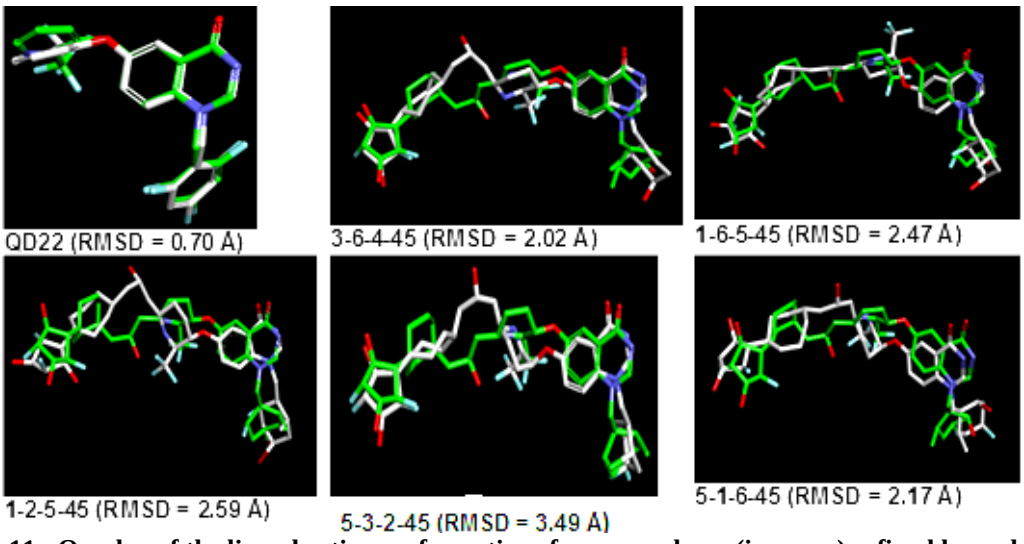

Figure 11: Overlay of the ligand active conformations from complexes (in green) refined by molecular mechanics and averaged active conformations (in white) resulting from MD simulations.

Table 8: Variation of the binding free energy ($\Delta\Delta G_{MM-GBSA}$) of the analogues.

Analogue	$\Delta\Delta H_{MM}$ [kcal.mol^{-1}]	$\Delta\Delta G_{solv}$ [kcal.mol^{-1}]	$T\Delta\Delta S_{vib}$ [kcal.mol^{-1}]	$\Delta\Delta G_{com}$ [kcal.mol^{-1}]	$\Delta\Delta G_{MM-GBSA}$ [kcal.mol^{-1}]	IC_{50}^{pre} [nM]
QD22 (ref)	0	0	0	0	0.00	60*
3-6-4-45	6.04	4.71	20.6	-16.75	-19.87	0.62
1-6-5-45	6.27	4.57	27.3	-16.46	-21.32	0.7
4-1-3-45	4.49	3.95	24.78	-16.35	-16.60	0.73
1-2-5-45	4.35	5.12	25.69	-16.22	-20.42	0.77
5-3-2-45	-0.32	4.18	20.06	-16.2	-20.02	0.78
5-1-6-45	3.73	5.66	18.65	-16.17	-20.81	0.79
2-1-6-45	2.7	6.85	18.06	-15.41	-21.81	1.07
1-4-6-45	3.98	6.67	18.53	-14.78	-10.92	1.39
1-3-4-45	4.76	5.39	17.72	-14.48	-5.74	1.57
1-6-3-45	7.59	4.94	19.87	-14.25	-10.92	1.73
1-2-6-45	2.95	8.02	18.02	-13.96	-14.25	1.94
2-6-4-45	5.89	6.67	19.5	-13.85	-23.92	2.03
6-3-3-45	3.47	5.95	16.34	-13.82	-4.03	2.05
5-6-1-45	4.72	6.05	17.17	-13.3	-24.54	2.54
6-3-4-45	6.58	5.74	18.29	-12.87	-9.29	3.02

*: Experimental IC_{50}^{exp} of QD22, the most active of the training set.

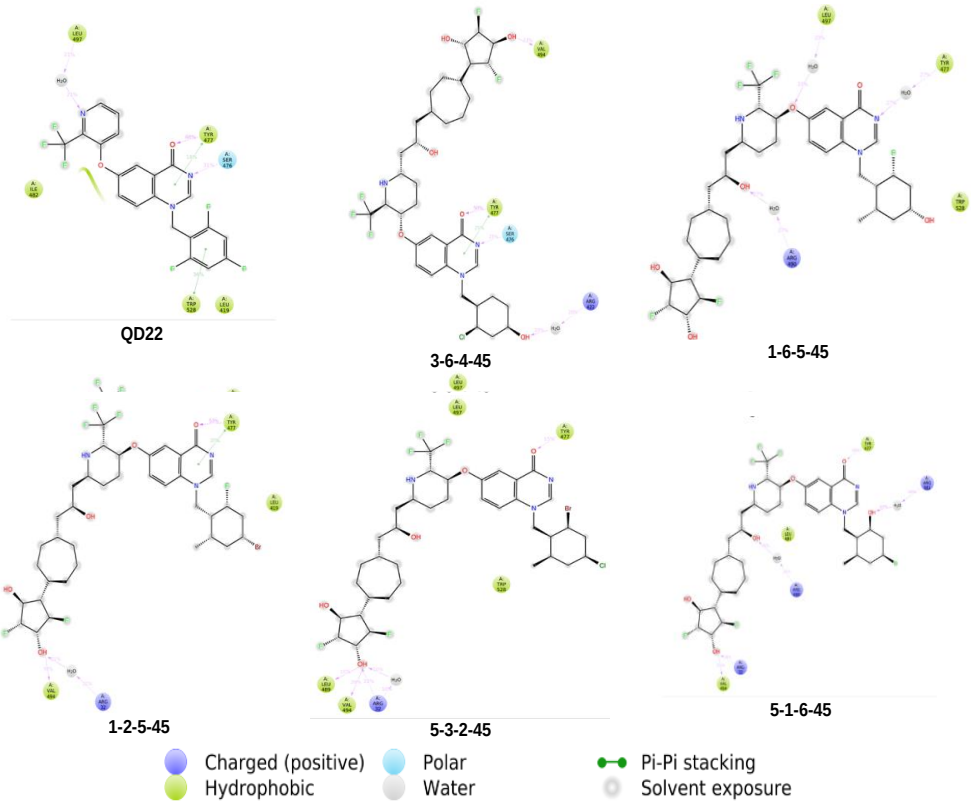

Figure 12: 2D representation of the most populated attractive interactions between the function groups of the QD22 and five new inhibitors and the individual residues at the active site of ns5b that occur in at least in 1/5 of the 500 analyzed frames.

The CF3 group contributes through halogen bonds with Val485 and Ala486. Two additional hydrogen bonds stabilize the extremities of the molecule via Leu497 and Arg498, while alkyl/π-alkyl contacts (Leu497, Ile482, Leu419) and hydrophobic interactions of the chlorine atom with Arg501 and Trp528 complete the network. Weak carbon-hydrogen bonds with Pro496 and His475 further refine the stabilization. This multivalent interaction network accounts for the high theoretical affinity of this analogue for NS5B.

To validate the obtained results, the relative MM-GBSA binding free energy calculated directly from the molecular dynamics simulation trajectories was compared to the relative Gibbs free energy of complexation[54]. The biological activities are within the same order of magnitude, as are each of the two thermodynamic quantities (Table 8). This convergence confirms the reliability of the computational approaches and allows us to propose these designed analogues as potential inhibitors.

Limitations of the study

Several limitations bound this work: the QSAR model's predictions are strictly restricted to the chemical space of its defined applicability domain; the validation metrics are inherently retrospective and may not perfectly mirror prospective experimental success; the statistical significance does not inherently guarantee a physical or biological causal mechanism; and the model's ultimate accuracy remains fundamentally capped by the baseline experimental noise and error present in the initial training data.

CONCLUSIONS

To characterize the inhibition of NS5B by quinazolinone derivatives (QDs), the X-ray crystal structure of the NS5B-QD14 complex was utilized. This approach demonstrated a strong correlation between the theoretical Gibbs free energies (GFE) and experimental inhibition data. These findings enabled the development of a 3D-QSAR pharmacophore (PH4) model, which was trained on 24 compounds and validated on 8 additional compounds. By examining the key interactions within the active site, a virtual chemical library of QD analogues was generated through targeted substitutions. This library was then filtered based on ADME criteria and mapped onto the PH4 model to ensure the bioavailability of the molecules. Finally, the properties of the top 15 virtual candidates were calculated using the QSAR model. These analogues represent strong candidates for the inhibition of NS5B polymerase.

ACKNOWLEDGEMENTS

The authors gratefully acknowledge Prof. Paola Gramatica for granting a free license for the QSARINS software.

AUTHOR'S CONTRIBUTIONS

Yavo BU: conception, final drafting, writing original manuscript. **Esmel AE:** conception, investigations, technical, computational coaching, software, editing.

Kouakou KJL: conception, investigations, computing, and editing. **Kéita M:** conception, intellectual input and final manuscript editing. **Eugène M:** intellectual input and final manuscript editing. Final manuscript was checked and approved by all authors.

DATA AVAILABILITY

The associated author can provide the empirical data used to support the study's conclusions upon request.

CONFLICT OF INTEREST

None to declare.

REFERENCES

1. Spearman C. Wendy, Dusheiko GM, Hellard M, *et al.* Hepatitis C. Lancet 2019.
2. OMS. Global hepatitis report 2024: action for access in low- and middle-income countries.
3. Pawlotsky JM. Hepatitis C Virus Resistance to Direct-acting antiviral drugs in interferon-free regimens. Gastroenter 2016;151(1):70–86. *https://doi.org/10.1053/j.gastro.2016.04.003*
4. Vaishali M. Patil Satya PG. Structural flexibility in HCV NS5B polymerase and molecular modelling of anti-HCV drugs . Curr C Bio 2018; 65–67.
5. Moradpour D, Penin F, Rice CM. Replication of hepatitis C virus. Nat Rev Microbio 2007;5(6):453–463. *https://doi.org/10.1038/nrmicro1645*
6. Powdrill MH, Bernatchez JA, Götte M, *et al.* Inhibitors of the hepatitis C virus RNS-dependent RNA polymerase NS5B. Viruses 2010; 2(10): 2169–2195. *https://doi.org/10.3390/v2102169*
7. Gillian M. Keating. Sofosbuvir: A Review of its use in patients with chronic Hepatitis C. Drugs 2014;74:1127-1146. *https://doi.org/10.1007/s40265-014-0247-z*
8. Sallamn M, Khalil R. Contemporary insights into hepatitis c virus: A comprehensive review. Microorganisms 2024;12:6. *https://doi.org/10.3390/microorganisms12061035*
9. Brigham D, Narkewicz MR. Profile of Sofosbuvir and Velpatasvir Combination in the treatment of chronic Hepatitis C in children and adolescents: Current evidence. in therapeutics and clinical risk management 2024;20:1–7. *https://doi.org/10.2147/TCRM.S326099*
10. Jácome R, Campillo-Balderas JA, Ponce de León S, *et al.* Sofosbuvir as a potential alternative to treat the SARS-CoV-2 epidemic. Sci Rep 2020;10(1):1–5. *https://doi.org/10.1038/s41598-020-66440-9*
11. Eltahla AA, Luciani F, White PA, *et al.* Inhibitors of the hepatitis C virus polymerase; mode of action and resistance. Viruses 2015;7(10):5206–5224. *https://doi.org/10.3390/v7102868*
12. Di Marco L, Cannova S, Ferrigno E, *et al.* A comprehensive review of antiviral therapy for hepatitis C: The long journey from interferon to pan-genotypic direct-acting antivirals (DAAs). Viruses 2025;17:2. *https://doi.org/10.3390/v17020163*
13. Sun D, Gao W, Hu H, Zhou S. Why 90% of clinical drug development fails and how to improve it? Acta Pharm Sin B. 2022;12(7):3049–62. *https://doi.org/10.1016/j.apsb.2022.02.002*
14. Yeung KS, Beno BR, Parcella K, *et al.* Discovery of a Hepatitis C Virus NS5B replicase palm site allosteric inhibitor (BMS-929075) advanced to Phase 1 clinical studies. J Med Chem 2017 May 25;60(10):4369–85. *https://doi.org/10.1021/acs.jmedchem.7b00328*
15. Beaulieu PL, Coulombe R, Duan J, *et al.* Structure-based design of novel HCV NS5B thumb pocket 2 allosteric inhibitors with submicromolar gt1 replicon potency: Discovery of a quinazolinone chemotype. Bioorg and Med Chem Lette 2013;23(14):4132–4140. *https://doi.org/10.1016/j.bmcl.2013.05.037*
16. Biovia DS. Discovery Studio Modeling Environment (2016). Dassault Systèmes.
17. Accelrys Inc. (2005). Insight-II and Discover molecular modeling and simulation package (2005 ed.). Accelrys, Inc.
18. Wu Z, Chen S, Wang Y, *et al*. Current perspectives and trend of computer-aided drug design: A review and bibliometric analysis. Int J Surg (London, England) 2024;110(6):3848–3878. *https://doi.org/10.1097/JS9.0000000000001289*
19. Adama N, Alex AYJ, Bernard DAM, *et al*. Study by molecular docking of the interactions between Dihydroorotate Dehydrogenase and a series of inhibitors of pyrrole derivatives for the treatment of malaria. Asian J Chem Sci 2025;15(1):92–110. *https://doi.org/10.9734/ajocs/2025/v15i1352*
20. Frecer V, Berti F, Benedetti F, *et al*. Design of peptidomimetic inhibitors of aspartic protease of HIV-1 containing -PheΨPro- core and displaying favourable ADME-related properties. J Mol Graph and Modelli 2008;27(3): 376–387. *https://doi.org/10.1016/j.jmgm.2008.06.006*
21. Vergara PS, Marucho M. MPBEC, a Matlab program for biomolecular electrostatic calculations. Phy Commu 2016; 198, 179–194. *https://doi.org/10.1016/j.cpc.2015.08.029*
22. Eugene M, Esmel A, Keita M, *et al*. Insight into binding mode of nitrile inhibitors of *Plasmodium falciparum* Falcipain-3, QSAR and Pharmacophore models, virtual design of new analogues with favorable pharmacokinetic profiles. SDRP J Comput Chem Mol Modelli 2017; 2(1). *https://doi.org/10.25177/jcmp.2.1.5*
23. King E, Aitchison E, Li H, *et al*. Recent developments in free energy calculations for drug discovery. In Frontiers in Molecular Biosciences 2021;8. *https://doi.org/10.3389/fmolb.2021.712085*
24. Wang B, Li L, Hurley TD, *et al*. Molecular recognition in a diverse set of protein-ligand interactions studied with molecular dynamics simulations and end-point free energy calculations. J Chem Inf and Model 2013;53(10):2659–2670. *https://doi.org/10.1021/ci400312v*
25. Kumar H, Datusalia A K, Khatik GL, *et al*. Virtual screening of acetylcholinesterase inhibitors through pharmacophore-based 3D-QSAR modeling, ADMET, molecular docking, and MD simulation studies. Silico Pharmacol 2024;12(1). *https://doi.org/10.1007/s40203-024-00189-1*
26. Bieri C, Esmel A, Keita M, *et al*. Structure-Based Design and pharmacophore-Based virtual screening of combinatorial library of Triclosan analogues active against Enoyl-Acyl carrier protein reductase of *Plasmodium falciparum* with favourable ADME profiles. Int J Molec Sci 2023;24(8). *https://doi.org/10.3390/ijms24086916*
27. Schrödinger. (2019). No Title.
28. Erin M. Duffy, William L. Jorgensen. Prediction of Properties from simulations: Free energies of Solvation in hexadecane, octanol, and water. J of the Ameri Chem Soc 2000;122(12):2878–2888.
29. Roméo NG, Yvon BMB, Bernard DAM, *et al.* Molecular modeling and virtual screening: Application to computer-aided design of anticancer inhibitors of human dihydroorotate dehydrogenase. J Pharm 2025;37(8):52–80. *https://doi.org/10.9734/jpri/2025/v37i87734*
30. Allangba KNPG, Keita M, Kre N'Guessan, *et al*. Virtual design of novel *Plasmodium falciparum* cysteine protease falcipain-2 hybrid lactone–chalcone and isatin–chalcone inhibitors probing the S2 active site pocket. J Enzy Inhibit and Med Chem 2019; 34(1): 547–561. *https://doi.org/10.1080/14756366.2018.1564288*
31. Daniel F. Veber, Stephen R. Johnson, Hung-Yuan Cheng, *et al*. Molecular properties that influence the oral bioavailability of drug candidates. J Med Chem 2002; 45(12).
32. Keïta M, Yaya Y, Bisseyou Yvon BM, *et al*. Molecular and thermodynamic modeling of the protein-ligand interaction. application to computer-assisted design of anti-competitive inhibitors of human histone deacetylase 2 (HDAC2). SDRP-J Comput Chem Mol Mod 2022; 605–630. *https://doi.org/10.25177/jccmm.5.2.ra.10763*
33. Bléhoué IC, Koné M, Esmel EA, *et al*. Molecular modeling and virtual screening application to the computer-aided design of anticancer inhibitors with a favorable pharmacokinetic profile against e6 papillomavirus type 16. Universal J Pharm Res 2024;9(5). *https://doi.org/10.22270/ujpr.v9i5.1198*

34. Frecer V, Miertus S. Antiviral agents against COVID-19: structure-based design of specific peptidomimetic inhibitors of SARS-CoV-2 main protease. RSC Adv 2020;10(66):40244–63. *https://doi.org/10.1039/D0RA08304F*
35. Schrödinger LLC, & D. E. Shaw Research. Desmond Molecular Dynamics System (3.6). Schrödinger, LLC 2018.
36. Devleena SK, Joshua W, Yujie W, *et al*. Prediction of absolute solvation free energies using molecular dynamics free energy perturbation and the OPLS force field. J Chem Theo and Computat 2010; 6(5).
37. Gramatica P, Cassani S, Roy PP, Kovarich S, Yap CW, Papa E. QSAR Modeling is not "Push a button and find a correlation": A case study of toxicity of (Benzo-)triazoles on Algae. Mol Inform 2012 Dec 1;31(11–12):817–35. *https://doi.org/10.1002/minf.201200075*
38. Gramatica P, Chirico N, Papa E, *et al*. QSARINS: A new software for the development, analysis, and validation of QSAR MLR models. J Comp Chem 2013; 34(24): 2121–2132. *https://doi.org/https://doi.org/10.1002/jcc.23361*
39. Gramatica P, Cassani S, Chirico N, *et al*. QSARINS-chem: Insubria datasets and new QSAR/QSPR models for environmental pollutants in QSARINS. J Computat Chem 2014;35(13):1036–1044. *https://doi.org/https://doi.org/10.1002/jcc.23576*
40. Gramatica P, Sangion A. A historical excursus on the statistical validation parameters for QSAR models: A clarification concerning metrics and terminology. J Chem Inf Model 2016 Jun 27;56(6):1127–31. *https://doi.org/10.1021/acs.jcim.6b00088*
41. Gramatica P. Principles of QSAR Modeling: Comments and suggestions from personal experience. Int J Quant Structure-Prop Relation 2020;5(3):61–97. *https://doi.org/10.4018/IJQSPR.20200701.oa1*
42. Gramatica P. Origin of the OECD Principles for QSAR validation and their role in changing the QSAR paradigm worldwide: An historical overview. J Chemom 2025 Mar 1;39(3):e70014. *https://doi.org/10.1002/cem.70014*
43. Chirico N, Sangion A, Gramatica P, *et al*. QSARINS-Chem standalone version: A new platform-independent software to profile chemicals for physico-chemical properties, fate, and toxicity. In J Comput Chem 2021;42:20. *https://doi.org/https://doi.org/10.1002/jcc.26551*
44. Muratov E N, Bajorath J, Sheridan R P, *et al.* QSAR without borders. Chem Soc Rev 2020; 49(11):3525–3564. *https://doi.org/10.1039/d0cs00098a*
45. Kouman KC, Kouassi AF, Fagnidi YKH, *et al.* Virtual design of novel of orally bioavailable piperazine inhibitors of enoyl-acyl carrier protein reductase of *Mycobacterium tuberculosis* with favorable pharmacokinetic profiles. Universal J Pharm Res 2024; 9(5): 91-104. *http://doi.org/10.22270/ujpr.v9i5.1216*
46. Kouassi AF, Kone M, Keita M, *et al*. Computer-aided design of orally bioavailable pyrrolidine carboxamide inhibitors of enoyl-acyl carrier protein reductase of Mycobacterium tuberculosis with favorable pharmacokinetic profiles. Int J Mol Sci 2015;16(12):29744–71. *http://doi.org/10.3390/ijms161226196*
47. Accelrys Inc. Discovery Studio molecular modeling and simulation program. 2.5. Accelrys, Inc.; 2009.
48. Lipinski CA, Lombardo F, Dominy BW, Feeney PJ. Experimental and computational approaches to estimate solubility and permeability in drug discovery and development settings. Adv Drug Deliv Rev 1997;23(1):3–25. *https://doi.org/10.1016/S0169-409X(96)00423-1*
49. James C. Phillips, David J. Hardy, Julio D. C. Maia, *et al.* Scalable molecular dynamics on CPU and GPU architectures with NAMD. J Chem Phy 2020;153(4):044130.
50. Rana N, Solanki P, Mehra R, Manhas A. Identification of natural compound inhibitors for substrate-binding site of MTHFD2 enzyme: Insights from structure-based drug design and biomolecular simulations. Chem Physics Impact 2025;10:100809. *https://doi.org/10.1016/j.chphi.2024.100809*
51. Oliver Hucke, René Coulombe, Pierre Bonneau, *et al.* Molecular dynamics simulations and structure-based rational design lead to allosteric HCV NS5B polymerase thumb pocket 2 Inhibitor with picomolar cellular replicon potency. J Med Chem 2013;57(7). *https://doi.org/10.1021/jm4004522*
52. Marina M. May, Dirk Brohm, Axel Harrenga, *et al*. Discovery of substituted N-phenylbenzenesulphonamides as a novel class of non-nucleoside hepatitis C virus polymerase inhibitors. Antivir Res 2012;95(2):182-191. *https://doi.org/10.1016/j.antiviral.2012.04.008*
53. Biswal, B, K, Wang M, cherney MM, *et al*. Non-nucleoside Inhibitors binding to Hepatitis C Virus NS5B Polymerase reveal a novel mechanism of inhibitin. Journal of Molecular Biol 2006;361(1): 33-45. *https://doi.org/10.1016/j.jmb.2006.05.074*
54. Gloua SM, Esmel AE, Zoro EGH, *et al*. Molecular modeling and virtual screening for computer-aided design of plant protoporphyrinogen IX oxidase (PPO) inhibitors. Sci Afr 2026; 31: e03208. *https://doi.org/https://doi.org/10.1016/j.sciaf.2026.e03208*